Spin-spin coupling in electrostatically coupled quantum dots

Mircea Trif, Vitaly N. Golovach, and Daniel Loss
Department of Physics and Astronomy, University of Basel, Klingelbergstrasse 82, CH-4056 Basel, Switzerland
(Received 23 August 2006; revised manuscript received 27 November 2006; published 7 February 2007)

We study the spin-spin coupling between two single-electron quantum dots due to the Coulomb and spin-orbit interactions, in the absence of tunneling between the dots. We find an anisotropic *XY* spin-spin interaction that is proportional to the Zeeman splitting produced by the external magnetic field. This interaction is studied both in the limit of weak and strong Coulomb repulsion with respect to the level spacing of the dot. The interaction is found to be a nonmonotonic function of interdot distance a_0 and external magnetic field and, moreover, vanishes for some special values of a_0 and/or magnetic field orientation. This mechanism thus provides a new way to generate and tune spin interaction between quantum dots. We propose a scheme to measure this spin-spin interaction based on the spin-relaxation-measurement technique.

DOI: 10.1103/PhysRevB.75.085307 PACS number(s): 73.21.La, 73.23.Hk, 73.63.Kv

I. INTRODUCTION

The spin degree of freedom of electrons in semiconductor nanostructures has attracted much interest recently. In addition to its applications in spintronics,[1] which makes use of the spin in the same way as the charge in conventional devices, there has been considerable interest in the quantum coherence of spin in different materials and geometries at the nanoscale.[2] The long coherence times measured some time ago in semiconductors[3] supported the idea of quantum computing with spins localized in quantum dots[4,5]—a rapidly growing field now, where recent experimental progress has been remarkable.[6–13]

Electron spins in semiconductor nanostructures, however, are not decoupled from the charge degree of freedom, one of the primary reasons for this coupling being the spin-orbit interaction. This coupling leads to many interesting phenomena in the physics of semiconductors,[1,2] an important one being the ability to control the spin of the electron with electric fields acting on its charge degrees of freedom.[14–19] In GaAs quantum dots the spin-orbit interaction manifests itself as a weak perturbation when compared with the confinement energy. The measure of smallness is given by the ratio between the dot radius λ and the spin-orbit length λ_{SO}—the distance over which an electron travels and thereby precesses its spin by an angle π about the intrinsic "magnetic" field induced by the spin-orbit interaction. We mention that there are also materials which possess large spin-orbit couplings, with the spin-orbit length on the same order as the dot size, e.g., InAs, InP quantum dots. Despite its smallness the spin-orbit interaction is very important for the coherence of the spin dynamics. For example, spin-orbit interaction allows for coupling of the electron spin to bosonic environments, such as phonons[20,21] or particle-hole excitations in quantum point contacts,[22] which in turn causes relaxation and decoherence of the spins. Moreover, electrons being charged particles interact via the long range Coulomb forces with each other, even if they are confined to well-separated quantum dots with no overlap of their wave functions. Through this electrostatic coupling and in combination with the spin orbit interaction, the spins of two electrons located in different dots become coupled even in the absence of tunneling between the dots.

In this paper we provide a detailed analysis of such an effective spin-spin interaction for lateral quantum dots in a configuration as shown in Fig. 1. We will see that the origin of this interaction is the "tidal" effect each of the electrons produces on the charge distribution of the other electron via electrostatic forces. Because of the spin-orbit interaction, the electric dipole moment (as well as higher moments) in each dot couples to its electron spin. As a result, the two spins experience an interaction resembling a magnetic dipole-dipole interaction[23] with effective magnetic moments which can be strongly enhanced by up to a factor of 10^3 compared to the Bohr magneton. The magnitude of the spin-spin coupling obtained via this spin-electric effect can be efficiently controlled and even completely suppressed by adjusting external parameters such as the magnetic field direction, strength, and interdot distance.

The spin-spin interaction can, in principle, be used to perform two-qubit operations as required in the spin-based quantum computing scheme,[4] because it entangles spins and can easily be switched on and off. We note that a similar

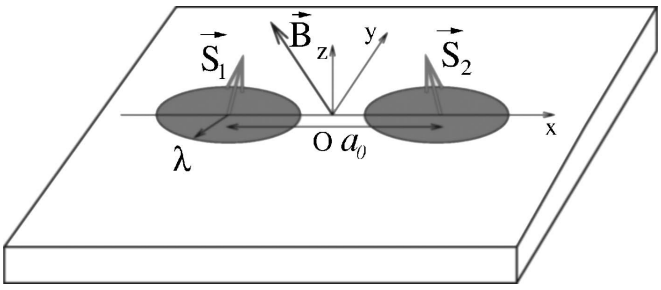

FIG. 1. The figure shows a sketch of the model system which consists of two identical quantum dots in the *xy* plane, separated by distance a_0 (measured from dot center to dot center). $\vec{S}_i$ denotes the spin of electron $i=1,2$, λ is the dot radius, and $\vec{B}$ is the external magnetic field. The respective orbital wave functions of electron 1 and 2 are assumed to have no overlap (i.e., tunneling between the dots is excluded). The remaining purely electrostatic Coulomb interaction between the electron charges leads, via spin-orbit interaction, to an effective coupling between their spins. This spin-spin interaction depends sensitively on the orientation of $\vec{B}$, with no component along it, and is proportional to $\vec{B}^2$.

mechanism for spin interaction based on electrostatic coupling was studied very recently in Ref. 24 for vertically coupled quantum dots, and in Ref. 25 for the special case of one-dimensional quantum dots formed in semiconducting nanowires. In addition to the differences in geometry and dimensionality, both of these works treat only the case of weak Coulomb interaction (compared to the level spacing), while we treat here also the opposite limit of strong Coulomb interaction where new and interesting features emerge. In the limiting case of strongly elliptical dots we recover the one-dimensional results obtained in Ref. 25.

We emphasize again that in the present study we exclude tunneling and thus the type of spin interaction studied in the following is fundamentally different from the Heisenberg exchange interaction for which the presence of electron tunneling between the dots is crucial.[26–29] Similarly, the combined effect of Heisenberg exchange interaction and spin-orbit coupling[30–34] is also based on tunneling and should be carefully distinguished from the spin-orbit effect studied here. We also note that the Heisenberg exchange coupling allows typically for much stronger spin-spin coupling than the electrostatically induced one. For instance, in GaAs dots the Heisenberg exchange can reach values on the order of 0.1–1 meV, which, as we shall see, exceeds the electrostatically induced spin coupling by three to four orders of magnitude. Nevertheless, the electrostatic spin-spin coupling can prove useful for cases where it is difficult to get sufficient wave function overlap (needed for large Heisenberg exchange), and, moreover, it is also important to understand the electrostatic spin effects in detail in order to get control over possible interference effects between different types of spin coupling. This will be for example of importance for spin qubit applications in order to minimize spin decoherence and gate errors.

Finally, in view of experimental tests we propose a scheme to measure the spin-spin interaction in a double dot setup with a nearby charge detector. We propose to combine the spin-measurement technique of Ref. 8 with the entangling property of the spin-spin interaction and present a gate pulsing sequence that enables one to access the coupling constant in the time domain by measuring the occupation probability of a Zeeman sublevel.

The paper is organized as follows. In Sec. II we introduce our model for the quantum-dot system and its basic Hamiltonian. In Sec. III we derive the effective spin-spin coupling Hamiltonian within our model. In this section we analyze in detail the two limiting cases of weak and strong Coulomb interaction, and obtain various forms of the spin coupling as function of magnetic field strength and orientation, as well as of the interdot distance. The most general form of the spin coupling tensor is given in the Appendix. In Sec. IV, we propose a scheme to measure the spin-spin coupling. There, we also discuss the effect of the hyperfine interaction with the nuclear spins on the measurement scheme. Finally, in Sec. V we discuss our results and end with some conclusions.

II. THE MODEL

Our system consists of two electrons each of which is localized in a quantum dot, and the two dots are separated from each other, without tunneling between them. The system is composed of two gate-defined quantum dots in a two-dimensional semiconductor layer (e.g., GaAs or InAs). A schematics of the system we consider is shown in Fig. 1.

We model the system by a harmonic confinement potential, which, for simplicity is assumed to be the same for both dots. Each dot is assumed to contain one electron with charge $-e$ and spin $\boldsymbol{S}=(\hbar/2)\boldsymbol{\sigma}$, with $\boldsymbol{\sigma}=(\sigma_x,\sigma_y,\sigma_z)$ being the Pauli matrices. The model Hamiltonian consisting of several terms reads

$$H = H_0 + H_Z + H_C + H_{\mathrm{SO}}, \tag{1}$$

where H_0 is the energy of the two electrons in the confinement potentials

$$H_0 = \sum_{i=1,2} \left(\frac{p_i^2}{2m^*} + U(\boldsymbol{r}_i) \right). \tag{2}$$

Here, $\boldsymbol{p}_i=-i\hbar\partial/\partial\boldsymbol{r}_i+(e/c)\boldsymbol{A}(\boldsymbol{r}_i)$ is the 2D kinetic momentum of the ith electron at position $\boldsymbol{r}_i$, m^* the effective mass, c the speed of light, $U(\boldsymbol{r}_i)=(m^*/2)\omega_0^2 r_i^2$ the confinement potential for the ith electron which is assumed to be harmonic and isotropic, and $\boldsymbol{A}(\boldsymbol{r}_i)$ is the electromagnetic vector potential. The strength of the confinement energy is given by the frequency ω_0. The second term on the right-hand side of Eq. (1) is the Zeeman energy of the two electrons

$$H_Z = \frac{1}{2} g \mu_B \boldsymbol{B}(\boldsymbol{\sigma}_1 + \boldsymbol{\sigma}_2). \tag{3}$$

The third term in Eq. (1) is the unscreened Coulomb interaction between the two electrons

$$H_C = \frac{e^2}{\kappa|\mathbf{r}_1 - \mathbf{r}_2 + \mathbf{a}_0|}, \tag{4}$$

where κ is the dielectric constant of the material and a_0 is the geometric distance between the two dots, namely between the potential minima ("center") of the dots. With this choice, we measure the distance for each electron from its own dot center. The last term in Eq. (1) is the spin-orbit coupling which for strong z confinement is given by

$$H_{\mathrm{SO}} = \sum_{i=1,2} [\beta(-p_x^i\sigma_x^i + p_y^i\sigma_y^i) + \alpha(p_x^i\sigma_y^i - p_y^i\sigma_x^i)], \tag{5}$$

being the sum of the Dresselhaus term[35] (β) which comes from bulk inversion asymmetry and the Rashba term[36] (α) coming from structure inversion asymmetry. We assume the same coefficients β and α for both dots. It is convenient to work with center-of-mass and relative coordinates,[37] as the Coulomb interaction couples only to the relative ones and the solution of the center-of-mass part is straightforward.[38,39] This then involves the standard substitutions $M=2m^*$, $m=m^*/2$, $\boldsymbol{R}=(\boldsymbol{r}_1+\boldsymbol{r}_2)/2$, $\boldsymbol{r}=\boldsymbol{r}_1-\boldsymbol{r}_2$, and $\boldsymbol{P}=\boldsymbol{p}_1+\boldsymbol{p}_2$ and $\boldsymbol{p}=(\boldsymbol{p}_1-\boldsymbol{p}_2)/2$.

III. SPIN-SPIN COUPLING

We now turn our attention to the spin-orbit interaction. As was shown in Ref. 21, the spin-orbit coupling gives non-zero

first order effects only if a magnetic field is present, as a consequence of the Kramers degeneracy. In order to describe the effective first order spin-orbit term in the presence of a magnetic field we make use of the Schrieffer-Wolff (unitary) transformation[19,21]

$$\tilde{H} = e^{S}(H_d + H_Z + H_{\mathrm{SO}})e^{-S} = H_d + \Delta H + e^{S}H_Z e^{-S}, \quad (6)$$

where $S=-S^{\dagger}$ is chosen such that $\mathcal{P}\Delta H=\Delta H$, with the projector operator $\mathcal{P}$ satisfying $\mathcal{P}A=\Sigma_n A_{nn}|n\rangle\langle n|\,\forall A$, and $H_d|n\rangle = E_n|n\rangle$. The Hamiltonian $H_d=H_0+H_C$ (or $H_d=H_R+H_r+H_C$ in center-of-mass and relative coordinates). The Hamiltonian $\tilde{H}=H_d+\Delta H$ is diagonal in the basis of H_d and has the same energy spectrum as the Hamiltonian $H=H_d+H_{\mathrm{SO}}$. In first order of the spin-orbit interaction H_{SO} the transformation generator becomes $S=(1-\mathcal{P})L_d^{-1}H_{\mathrm{SO}}$, where L_d is the dot Liouvillean, $L_dA=[H_R+H_r+H_C,A]$, $\forall A$. Evaluating this expression explicitly we obtain

$$S = (1-\mathcal{P})i\sum_{i=1,2}\boldsymbol{\xi}_i\cdot\boldsymbol{\sigma}_i, \quad (7)$$

with $\boldsymbol{\xi}_{1,2}=(y_{1,2}/\lambda_+, x_{1,2}/\lambda_-, 0)$. In second order in spin-orbit coupling the transformed Hamiltonian $\tilde{H}$ becomes

$$\tilde{H} = H_R + H_r + H_Z + H_C + H_{\mathrm{SO}}^{Z} + \Delta H_{\mathrm{SO}}, \quad (8)$$

with $H_{\mathrm{SO}}^{Z}=H_{\mathrm{SO}}^{Z1}+H_{\mathrm{SO}}^{Z2}$ and $\Delta H_{\mathrm{SO}}=1/2[S,H_{\mathrm{SO}}]+[S,[S,H_Z]]$, where

$$H_{\mathrm{SO}}^{Z1,2} = [S,H_Z^{1,2}] = E_Z(1-\mathcal{P})[\boldsymbol{l}\times(\boldsymbol{\xi}_R \pm \boldsymbol{\xi}_r/2)]\boldsymbol{\sigma}_{1,2}, \quad (9)$$

$$\Delta H_{\mathrm{SO}} = \frac{\hbar}{m^{*}\lambda_-\lambda_+}(1-\mathcal{P})\sum_{i=1,2}(x_i p_{iy} - y_i p_{ix})\sigma_{iz} + E_Z\frac{1}{\lambda_-\lambda_+}(1-\mathcal{P})\sum_{i=1,2}[(\boldsymbol{l}\times\boldsymbol{\xi}_i)\times\boldsymbol{\xi}_i]\boldsymbol{\sigma}_i. \quad (10)$$

In Eqs. (9) and (10) $\boldsymbol{l}=\boldsymbol{B}/B$ is the magnetic field direction vector, $E_Z=g\mu_B B$ is the Zeeman energy and the vectors $\boldsymbol{\xi}_R$ and $\boldsymbol{\xi}_r$ are given by $\boldsymbol{\xi}_R=(Y'/\lambda_-, X'/\lambda_+, 0)$ and $\boldsymbol{\xi}_r=(y'/\lambda_-, x'/\lambda_+, 0)$, respectively. The new coordinates correspond to a rotation by an angle $\pi/4-\gamma$ with respect to the coordinate frame in which the direction of the $\boldsymbol{a}_0$ vector is associated with the x axis in the $XY(xy)$ plane so that the final expressions have the simplest form.[21] Here, γ is the angle between the xy frame in Fig. 1 and the normal axes of the crystal. The spin-orbit lengths $\lambda_{\pm}$ are given in the form $1/\lambda_{\pm}=m^{*}(\beta\pm\alpha)$. The terms which are of second order in spin-orbit coupling in Eq. (10) (which are also zero and first order, respectively, in Zeeman splitting) are single-spin terms and no coupling between spins take place in this order. In fact, they are just second order terms which are present in perturbation theory for an isolated spin in a QD, but now renormalized by the Coulomb interaction between the two electrons. We neglect these terms in the following analysis since they only change the on-site Zeeman interaction by a small amount. We are now in a position to derive the coupling between the two spins. This is achieved by performing a second Schrieffer-Wolff (SW2) transformation which excludes the first order contribution in spin-orbit interaction with no diagonal matrix elements. The new transformed Hamiltonian has the form $H_{\mathrm{eff}}=e^{T}\tilde{H}e^{-T}$, with T given by

$$T = (1-\mathcal{P})i(L_d + L_Z)^{-1}H_{\mathrm{SO}}^{Z}. \quad (11)$$

We assume now that the Zeeman energy is smaller than the orbital confining energy $E_Z \ll \hbar\omega_0$, which is usually the case for electrons in quantum dots, such that we can neglect in Eq. (11) the Zeeman Liouvillean L_Z (for spin-orbit effects due to level crossing see Ref. 40). In second-order in spin-orbit coupling the effective Hamiltonian H_{eff} becomes

$$H_{\mathrm{eff}} = H_d + H_Z + \frac{1}{2}[L_d^{-1}H_{\mathrm{SO}}^{Z}, H_{\mathrm{SO}}^{Z}]. \quad (12)$$

The last term in Eq. (12) contains the desired spin-spin coupling between the two spins. However, in addition to this interaction it also contains some self-interaction terms which renormalizes only the Zeeman splitting. We will not study those terms since they are of no practical interest in the case of identical dots. We consider a general magnetic field $\boldsymbol{B}=(\cos\Phi\sin\theta, \sin\Phi\sin\theta, \cos\theta)$, where θ is the angle between the magnetic field and the z axis perpendicular to the 2DEG plane and Φ the angle between the in-plane component of the magnetic field and the x direction (Fig. 1). The interaction between the two spins has the most general form

$$\tilde{H}_s = \frac{1}{2}\sum_{i\neq j}[L_d^{-1}H_{\mathrm{SO}}^{Zi}, H_{\mathrm{SO}}^{Zj}], \quad i,j=1,2. \quad (13)$$

The spin Hamiltonian is obtained by averaging over the orbital ground state $H_s=\langle 0|\tilde{H}_s|0\rangle$. We obtain

$$H_s = \boldsymbol{\sigma}_1\cdot\bar{\bar{M}}\boldsymbol{\sigma}_2, \quad (14)$$

where

$$\bar{\bar{M}}_{ab} = E_Z^2\langle 0|[(\boldsymbol{l}\times L_d^{-1}\boldsymbol{\xi}_1)_a, (\boldsymbol{l}\times\boldsymbol{\xi}_2)_b]|0\rangle \quad , a,b=x,y,z. \quad (15)$$

We note that there is no component of the spin along the magnetic field direction as a consequence of the vector product in the tensor $\bar{\bar{M}}$. By diagonalizing the above tensor, we obtain for the Hamiltonian H_s the reduced expression

$$H_s = J_{\tilde{x}}\sigma_{\tilde{x}}^1\sigma_{\tilde{x}}^2 + J_{\tilde{y}}\sigma_{\tilde{y}}^1\sigma_{\tilde{y}}^2, \quad (16)$$

where the couplings $J_{\tilde{x},\tilde{y}}$ depend on the magnetic field orientation and on the functions $C_{a_1b_2}=\langle 0|[L_d^{-1}a_1, b_2]|0\rangle$, with $a,b=x,y$ (for explicit expressions see the Appendix). Thus, the effective spin-spin interaction is highly anisotropic, and, in general, of the XY type. We note in particular that for an in-plane magnetic field ($\theta=\pi/2$), the spin Hamiltonian reduces to the Ising Hamiltonian $H_s=J_{\tilde{y}}\sigma_{\tilde{y}}^1\sigma_{\tilde{y}}^2$ (in a transverse magnetic field). Next, we rewrite H_s in terms of raising/lowering spin operators $\sigma_{\pm}=\sigma_{\tilde{x}}\pm i\sigma_{\tilde{y}}$

$$H_s = J_{\mathrm{eff}}(\sigma_+^1\sigma_-^2 + \sigma_-^1\sigma_+^2) + J'_{eff}(\sigma_-^1\sigma_-^2 + \sigma_+^1\sigma_+^2), \quad (17)$$

with $J_{\mathrm{eff}}=(1/2)(J_{\tilde{x}}+J_{\tilde{y}})$ and $J'_{\mathrm{eff}}=(1/2)(J_{\tilde{x}}-J_{\tilde{y}})$. We recall now that the *full* spin Hamiltonian includes the Zeeman en-

ergy, given in Eq. (3), which leads to a large energy gap with $2E_Z \gg J_{\tilde{x},\tilde{y}}$. We will find below that typically

$$\frac{J_{\tilde{x},\tilde{y}}}{E_Z} \sim \frac{E_Z}{\hbar\omega_0}\left(\frac{\lambda}{\lambda_{SO}}\right)^2 \ll 1 \tag{18}$$

under our assumption that $E_Z \ll \hbar\omega_0$ and $\lambda \ll \lambda_{SO}$. As a consequence, we can neglect in Eq. (17) the terms proportional to J'_{eff} since they cause transitions between different Zeeman levels of the total spin. The relevant spin-spin interaction H_s^{eff} which acts only within the $S-T_0$ subspace, becomes then

$$H_s^{\text{eff}} = J_{\text{eff}}(\sigma_+^1\sigma_-^2 + \sigma_-^1\sigma_+^2). \tag{19}$$

Thus, we are left with the task of calculating the coupling strengths $J_{\tilde{x},\tilde{y}}$ and J_{eff}. Because of the Coulomb term, (4), this cannot be done exactly and some approximations are required. They will depend on the ratio δ between the Coulomb interaction strength $e^2/\kappa a_0$ and the orbital level spacing $\hbar\omega_0$ giving $\delta=(e^2/\kappa a_0)/\hbar\omega_0=(\lambda/a_B)(\lambda/a_0)$, with $\lambda=\sqrt{\hbar/m^*\omega_0}$ being the dot radius and $a_B=\hbar^2\kappa/m^*e^2$ the Bohr radius in the material. In other words, the parameter δ will dictate the physics of the system, and from now on we will speak of the ratio λ/a_B as being the Coulomb interaction strength (representing in fact the "true" Coulomb strength for touching dots). For making the following analysis more transparent we focus on the case with only Rashba spin-orbit coupling ($\lambda_-=\lambda_+\equiv\lambda_{SO}$). The generalization to the case with both Rashba and Dresselhaus terms present is straightforward, but at the cost of more complicated expressions (see the Appendix).

A. Weak Coulomb coupling $\delta \ll 1$

One interesting case is met when $\delta \ll 1$, such that the Coulomb interaction can be treated as a perturbation compared to the orbital level spacing. In this case, one can retain only the first order contribution from the Coulomb interaction, which translates into the approximation $L_d^{-1} \approx L_0^{-1} - L_0^{-1}L_C L_0^{-1}$. Making use of this and after some algebra we obtain for the spin-spin coupling the following expression:

$$H_s = \int d\boldsymbol{r}_1 d\boldsymbol{r}_2 \frac{\delta\rho_1\delta\rho_2}{\kappa|\boldsymbol{r}_1 - \boldsymbol{r}_2 + \boldsymbol{a}_0|}, \tag{20}$$

where the operators $\delta\rho_i$, $i=1,2$, are the charge density distribution modifications in each dot as a consequence of the spin-orbit interaction. They are defined as

$$\delta\rho_i = \rho_i - \rho_i^0, \quad i=1,2, \tag{21}$$

with ρ_i^0 being the charge density operator in the absence of spin-orbit interaction and $\rho_i = e^{T_0}\rho_i^0 e^{-T_0}$ the one in the presence of spin-orbit interaction, with $T_0 = L_0^{-1}H_{SO}^Z$ for the present approximation. From Eq. (20) we see that the spin interaction results from a Coulomb-type of coupling between two charge density distributions which themselves depend on spin.

Let us now analyze in more detail Eq. (20). The first task is to find $\delta\rho_i$, for $i=1,2$, namely, the spin-orbit induced charge distribution or the spin-dependent charge distributions for each dot. In order to do this, we give first some important relations valid in the case of harmonic confining potential, relations which are used in the following for the derivation of the main results

$$L_0^{-1}x_i = -\frac{i}{\hbar m^*\omega_0^2}\left(p_x^i + \frac{eB_z}{c}y_i\right), \tag{22}$$

$$L_0^{-1}y_i = -\frac{i}{\hbar m^*\omega_0^2}\left(p_y^i - \frac{eB_z}{c}x_i\right), \tag{23}$$

$$L_0^{-1}\boldsymbol{p}_i = \frac{im^*}{\hbar}\boldsymbol{r}_i. \tag{24}$$

Making use of the relations (22)–(24) and within the first order of spin-orbit coupling, i.e., $\delta\rho_i \approx [T_0, \rho_i^0]$, we obtain

$$\delta\rho_i(\boldsymbol{r}) = \frac{2eE_Z}{m^*\lambda^2\omega_0^2\lambda_{SO}}\rho_{0i}[\cos\theta(y_i\cos\Phi + x_i\sin\Phi)\sigma_x^i + (y_i\sin\Phi - x_i\cos\Phi)\sigma_y^i], \tag{25}$$

with ρ_i^0 being the bare charge density in the dot corresponding to the ground state and which assumes the well-known form for harmonic potentials

$$\rho_i^0(\boldsymbol{r}) = \frac{1}{\pi\lambda^2}e^{-(x_i^2+y_i^2)/\lambda^2}. \tag{26}$$

We note that when there exist a perpendicular component of the magnetic field, the dot radius is renormalized due to the orbital effect of the magnetic field $\lambda \to \lambda(1+r^2)^{-1/4}$, with $r=\omega_0/2\omega_c$ ($\omega_c=eB_z/m^*c$, $B_z=B\cos\theta$). However, we will still refer to λ as being the dot radius, with the appropriate expression depending on the magnetic field orientation. We could now insert the expression (25) for $\delta\rho_i$ in Eq. (20) and compute directly the spin Hamiltonian. However, working with the Coulomb potential, it is more convenient to work with the center-of-mass and relative coordinates and for simplicity the x axis along the interdot direction $\boldsymbol{a}_0$. Assuming for simplicity a perpendicular magnetic field, the spin Hamiltonian H_s takes the form

$$H_s = \frac{4e^2E_Z^2}{m^{*2}\lambda^4\omega_0^4\lambda_{SO}^2}\int\int d\boldsymbol{r}d\boldsymbol{R}\rho_0(r)\rho_0(R) \times \frac{(X^2 - x^2/4)\sigma_x^1\sigma_x^2 + (Y^2 - y^2/4)\sigma_y^1\sigma_y^2}{\kappa\sqrt{y^2 + (x+a_0)^2}}, \tag{27}$$

with the electronic densities $\rho_0(r)=(2/\pi\lambda^2)\exp(-r^2/2\lambda^2)$ and $\rho_0(R)=(1/2\pi\lambda^2)\exp(-2R^2/\lambda^2)$. In Eq. (27) there are no mixed terms such as $\sigma_x^1\sigma_y^2$ since those terms vanish because of the odd symmetry of the integrands in the case of harmonic confinement, which reflects inversion symmetry. The limit of in-plane magnetic field is obtained very easy from Eq. (27) by substituting the denominator with $[(X^2 - x^2/4)\cos^2\Phi + (Y^2 - x^2/4)\sin^2\Phi]\sigma_y^1\sigma_y^2$. [For general field orientation the expression for H_s is more complicated (see the Appendix).] In order to make the following analysis more

transparent, we introduce the dimensionless coordinates $\boldsymbol{r}\rightarrow\boldsymbol{r}/\lambda$ and $\boldsymbol{R}\rightarrow\boldsymbol{R}/\lambda$. The integration over the center-of-mass coordinates is now straightforward and the reduced expression for the spin Hamiltonian becomes

$$H_s = \frac{E_Z^2}{m^{*2}\lambda^2\omega_0^4\lambda_{\mathrm{SO}}^2}(\Delta E_C^x \sigma_x^1\sigma_x^2 + \Delta E_C^y \sigma_y^1\sigma_y^2) \tag{28}$$

for a perpendicular magnetic field and

$$H_s = \frac{E_Z^2}{m^{*2}\lambda^2\omega_0^4\lambda_{\mathrm{SO}}^2}(\Delta E_C^x \sin^2\Phi + \Delta E_C^y \cos^2\Phi)\sigma_{\tilde{y}}^1\sigma_{\tilde{y}}^2 \tag{29}$$

for an in-plane magnetic field oriented at an angle Φ with respect to the interdot distance vector $\boldsymbol{a}_0$. The energy differences $\Delta E_C^{x,y}$ are given by

$$\Delta E_C^x = \frac{e^2}{\kappa\lambda}\int d\boldsymbol{r}\rho_0(r)\frac{1-x^2}{\sqrt{y^2+(x+a_0/\lambda)^2}}, \tag{30}$$

$$\Delta E_C^y = \frac{e^2}{\kappa\lambda}\int d\boldsymbol{r}\rho_0(r)\frac{1-y^2}{\sqrt{y^2+(x+a_0/\lambda)^2}}. \tag{31}$$

The ground state and the first excited states of the dots in relative coordinates give rise to different charge distributions (ρ_0, ρ_{1x}, and ρ_{1y}, respectively), and thus to different potential energies seen by a test charge at a distance a_0 (along x) away from the center of the charge distribution (in relative coordinates). $\Delta E_C^{x,y}$ are the differences between these potential energies.

Before studying the distance dependence of the spin Hamiltonian H_s (determined by $\Delta E_C^{x,y}$) in the entire range of distances, it is instructive to see how the expression (20) behaves in the large distance limit $a_0 \gg \lambda$ and to make some comparison with the magnetic dipolar interaction in vacuum.[2] We perform a multipole expansion of the Hamiltonian in Eq. (20). The first nonzero contribution takes the form of a dipole-dipole interaction between two spin-dependent electric dipoles, or phrased differently, the interaction between two charge-induced magnetic dipoles

$$H_s \approx \frac{\boldsymbol{m}_1\cdot\boldsymbol{m}_2 - 3(\boldsymbol{m}_1\cdot\boldsymbol{n}_a)(\boldsymbol{m}_2\cdot\boldsymbol{n}_a)}{\kappa a_0^3}, \tag{32}$$

with the dipole moments $\boldsymbol{m}_i$ given by

$$\boldsymbol{m}_i = \mathrm{Tr}_{\mathrm{orb}}[\delta\rho_i\boldsymbol{r}_i] = \bar{\bar{\mu}}\boldsymbol{\sigma}_i, \quad i=1,2. \tag{33}$$

Here, the trace is taken over the orbital degrees of freedom with $\boldsymbol{n}_a=\boldsymbol{a}_0/a_0$ and $\bar{\bar{\mu}}$ being the tensor corresponding to an effective spin-orbit induced magneton

$$\bar{\bar{\mu}} = \frac{eE_Z}{m^*\omega_0^2\lambda_{\mathrm{SO}}}\begin{pmatrix} -\cos\theta & 0 & 0 \\ 0 & \cos\theta & 0 \\ 0 & \sin\theta & 0 \end{pmatrix}. \tag{34}$$

We see from Eq. (34) that the tensor $\bar{\bar{\mu}}$ depends on the magnetic field orientation with respect to the 2DEG and that it is also anisotropic, in contrast to the usual isotropic Bohr magneton $\mu_B=e\hbar/2m_ec$ (m_e is the mass of the free electron and c the speed of light). We note that the z component of the induced magnetic moment (with $\hat{\boldsymbol{z}}\|\boldsymbol{B}$) vanishes, i.e., $\boldsymbol{m}=(m_x,m_y,0)$. Let us quantify the strength of $\bar{\bar{\mu}}$ by the norm $\|\bar{\bar{\mu}}\|=(1/\sqrt{3})\sqrt{\Sigma_{i,j}\mu_{ij}^2}$, i.e.,

$$\|\bar{\bar{\mu}}\| = \frac{1}{\sqrt{3}}\frac{eE_Z}{m^*\omega_0^2\lambda_{\mathrm{SO}}}\sqrt{1+\cos^2\theta}. \tag{35}$$

We compare now $\|\bar{\bar{\mu}}\|$ with μ_B. First of all, we note that $\|\bar{\bar{\mu}}\|$ vanishes when there is no Zeeman splitting. However, for finite magnetic fields, $\|\bar{\bar{\mu}}\|$ can exceed μ_B by many orders of magnitude in the case of quantum dots. To give an estimate, we assume $\hbar\omega_0\approx 0.5$ meV, $E_Z\approx 0.05$ meV ($B\approx 2$ T) and $m^*=0.067m_e$, $\lambda_{\mathrm{SO}}\approx 10^{-6}$ m for GaAs quantum dots. With these values, and taking $\theta=0$ (perpendicular magnetic field) we obtain

$$\frac{\|\bar{\bar{\mu}}\|}{\mu_B} = \frac{4}{\sqrt{3}}\frac{E_Z}{\hbar\omega_0}\frac{m_e}{m^*}\frac{c}{\omega_0\lambda_{\mathrm{SO}}} \approx 10^3. \tag{36}$$

We describe now in more detail the limit of large distance between the dots. From Eqs. (28) and (27) we find for $a_0 \gg \lambda$

$$H_s = J(\sigma_y^1\sigma_y^2 - 2\sigma_x^1\sigma_x^2), \tag{37}$$

for a perpendicular magnetic field, and

$$H_s = J(\cos^2\Phi - 2\sin^2\Phi)\sigma_{\tilde{y}}^1\sigma_{\tilde{y}}^2 \tag{38}$$

for an in-plane magnetic field, with the coupling strength J having the form

$$J = \frac{e^2E_Z^2}{\kappa m^{*2}\omega_0^4\lambda_{\mathrm{SO}}^2 a_0^3}. \tag{39}$$

From Eq. (39) we see a large distance decay $\sim a_0^{-3}$, i.e., a long range type behavior. We note also that the large distance result in Eq. (39) does not depend anymore on the orbital effect of the magnetic field. Working instead with the effective Hamiltonian defined in Eq. (19), the effective coupling strength J_{eff} for arbitrary magnetic field is given by

$$J_{\mathrm{eff}} = -\frac{J}{2}[1+\sin^2\theta(1-3\sin^2\Phi)]. \tag{40}$$

We note that the spin coupling can range from maximally ferromagnetic interaction with $J_{\mathrm{eff}}=-J$ at $\theta=\pi/2$ and $\Phi=0$ to maximally antiferromagnetic interaction with $J_{\mathrm{eff}}=J/2$ at $\theta=\pi/2$ and $\Phi=\pi/2$, and with J_{eff} passing through zero for certain angles.

Next, we consider the case of arbitrary distance but still with small Coulomb interaction strength as defined at the beginning of this section. Considering H_s^{eff} defined in Eq. (19) we obtain

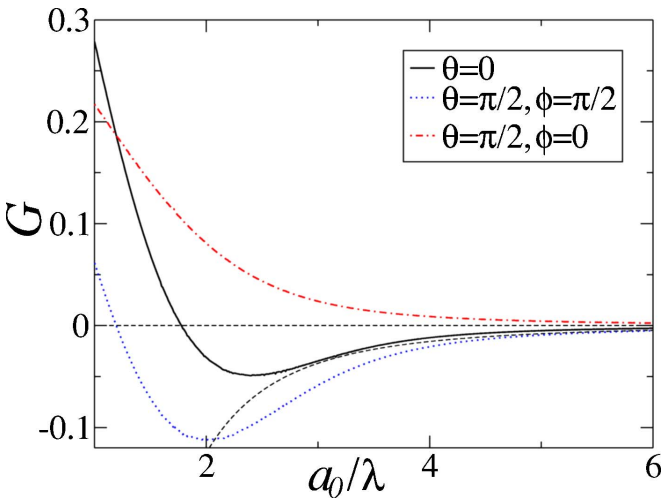

FIG. 2. (Color online) The function G occurring in Eq. (42) plotted as a function of the geometric distance a_0 between the dot centers scaled by the dot radius λ for different magnetic field orientations. The dashed line represents the dipolar approximation of G for a perpendicular magnetic field ($\theta=0$) which scales as a_0^{-3}.

$$J_{\text{eff}} = E_Z \frac{\lambda}{a_B} \frac{E_Z}{\hbar\omega_0} \left(\frac{\lambda}{\lambda_{\text{SO}}}\right)^2 G(a_0/\lambda, \theta, \Phi), \tag{41}$$

where

$$G(a_0/\lambda, \theta, \Phi) = \frac{\kappa\lambda}{e}[(\cos^2\theta\cos^2\Phi + \sin^2\Phi)\Delta E_C^y + (\cos^2\theta\sin^2\Phi + \cos^2\Phi)\Delta E_C^x]. \tag{42}$$

The function $G(a_0/\lambda, \theta, \Phi)$ is plotted in Fig. 2 for different angles θ and Φ. As for the large distance limit in Eq. (40), a similar but more complicated ferromagnetic-antiferromagnetic crossover behavior occurs as a function of the field orientation. However, in this case this behavior can also be induced by changing the distance between the dots a_0 (see Fig. 2).

Equation (41) suggests that the condition $\delta \ll 1$ is too restrictive. Instead, the weaker condition $(\lambda/a_B)(\lambda/a_0)^3 \ll 1$ is sufficient for the approximation to be valid. Figure 2 shows a breakdown of the dipolar approximation (i.e., of the a_0^{-3} decay), occurring at a dot separation $a_0/\lambda \approx 2$ for perpendicular magnetic fields ($\theta=0$), and also a cancellation of this interaction for some given distance, which is around $a_0/\lambda \approx 1.8$. This shows that the sum of the two electrostatic energy differences $\Delta E_C^x + \Delta E_C^y$ has a nonmonotonic behavior as a function of the distance a_0. Actually, only ΔE_C^x is nonmonotonic, whereas ΔE_C^y has a positive value which decreases with a_0, as can be seen from Fig. 2. If an in-plane magnetic field is applied along y ($\Phi=0$) or x ($\Phi=\pi/2$) direction, we obtain a dependence only either on ΔE_C^y or on ΔE_C^x. Accordingly, $G(a_0/\lambda)$ will be larger in some parameter range as compared with the case of perpendicular fields, see Fig. 2. At this point it is instructive to consider numerical estimates for the coupling strength J_{eff}. For this we consider GaAs quantum dots for which we assume $\lambda_{\text{SO}} \approx 10^{-6}$ m, $m^* = 0.067 m_e$, $g=-0.44$, $\kappa=13$, and also consider $\hbar\omega_0 \approx 0.5$ meV, $E_Z = 0.05$ meV ($B \approx 2$ T), and $a_0 = 5 \times 10^{-7}$ m. These estimations lead to a coupling strength $J \approx 10^{-10}$ eV, which lead to a time dynamics of the order of 10^{-5} s. If this time scale is longer than the decoherence times in GaAs quantum dots, the system will be insensitive to the coherent dynamics induced by the coupling J_{eff}. Shorter time scales are obtained for materials with larger spin-orbit coupling such as InAs. The spin-orbit length λ_{SO} in this material is comparable with a typical dot size of about 100 nm. Even though our perturbative approach starts to get unreliable in this case, it still can provide a rough estimate for the coupling strength. For InAs we have $m^* = 0.023 m_e$, $g=14.8$, $\kappa=13$, $\lambda_{\text{SO}} \approx 100$ nm, and we choose $\hbar\omega_0 \approx 1$ meV, $E_Z \approx 0.1$ meV, and $a_0/\lambda \approx 3$. With those values we obtain for the coupling $J_{\text{eff}} \approx 10^{-7}$ eV, which corresponds to a switching time of about ~ 50 ns for a swap of the spin states of electron one and electron two. This time scale for the spin dynamics is shorter than the expected spin decoherence time in such quantum dots. Thus, this interaction mechanism provides a useful way for the dynamical control of the spin-spin coupling. As discussed before, for an in-plane magnetic field the coupling constant could even be higher, depending on the angle of the magnetic field with respect to the interdot axis.

B. Elliptical dots with $\delta \ll 1$

We briefly generalize the previous results to elliptical dot shapes. This will also allow us to study the one-dimensional limit and recover previous results obtained for one-dimensional nanowires.[25] We consider elliptical dots which are characterized by the frequencies ω_{0x} and ω_{0y} corresponding to the x and y directions, respectively. In this case, Eq. (39) is replaced by

$$H_s = \frac{e^2 E_Z^2}{m^{*2}\lambda_{\text{SO}}^2} \left(\frac{\Delta E_C^x}{\omega_{0x}^4 \lambda_1^2} \sigma_x^2 \sigma_x^2 + \frac{\Delta E_C^y}{\omega_{0y}^4 \lambda_2^2} \sigma_y^1 \sigma_y^2 \right), \tag{43}$$

where the electrostatic energies $\Delta E_C^{x,y}$ become now

$$\Delta E_C^x = \frac{1}{\kappa\lambda_1} \int d\boldsymbol{r} \rho_0(\boldsymbol{r}) \frac{1 - x^2}{\sqrt{y^2 + (x + a_0/\lambda_1)^2}}, \tag{44}$$

$$\Delta E_C^y = \frac{1}{\kappa\lambda_2} \int d\boldsymbol{r} \rho_0(\boldsymbol{r}) \frac{1 - y^2}{\sqrt{y^2 + (x + a_0/\lambda_2)^2}}, \tag{45}$$

with the charge density distribution function, expressed in relative coordinates

$$\rho_0(\boldsymbol{r}) = \frac{2}{\pi\lambda_1\lambda_2} e^{-x^2/2\lambda_1^2 - y^2/2\lambda_2^2}. \tag{46}$$

For perpendicular magnetic fields and elliptical dots the lengths $\lambda_{1,2}$ are given by[41]

$$\lambda_{1,2} = \sqrt{\frac{4\hbar(n+1)}{m_{1,2}^* \omega_{1,2}}}, \tag{47}$$

where $n=m_1m_2\omega_1\omega_2\omega_c^2/B^2$, $\omega_{1,2}=\sqrt{A\pm B}/2$, $m_{1,2}=2B/(C\pm\omega_c^2+B)$, and $m_{1,2}^*=m_{1,2}m^*$ with the explicit expressions for A, B, and C

$$A=\omega_{0x}^2+\omega_{0y}^2+\omega_c^2, \tag{48}$$

$$B=\sqrt{(\omega_{0x}^2+\omega_{0y}^2+\omega_c^2)^2-4\omega_{0x}^2\omega_{0y}^2}, \tag{49}$$

$$C=\omega_{0x}^2-\omega_{0y}^2. \tag{50}$$

Taking now also the limit of strongly elliptical dots, i.e., $\omega_{0y}\gg\omega_{0x},\omega_c$, we see that this is equivalent to keeping only one component of the spin interaction, namely, the $\sigma_x^1\sigma_x^2$ part, and that the orbital effect of the magnetic field drops out. The resulting Hamiltonian then becomes

$$H_s=\frac{e^2E_Z^2\Delta E_C^x}{m^{*2}\omega_{0x}^4\lambda^2\lambda_{\mathrm{SO}}^2}\sigma_x^1\sigma_x^2+O[(\omega_{0x}/\omega_{0y})^4]. \tag{51}$$

Considering now the large distance limit, $a_0\gg\lambda$, analogously to Eq. (37), our result reduces formally to the one in Ref. 25, i.e.,

$$H_s=-2\frac{e^2E_Z^2}{\kappa m^{*2}\omega_{0x}^4\lambda_{\mathrm{SO}}^2a_0^3}\sigma_x^1\sigma_x^2+O[(\omega_{0x}/\omega_{0y})^4]. \tag{52}$$

The above expression (52) can be also obtained directly from Eq. (37) since within the considered limit there is no orbital effect of the perpendicular magnetic field on the spin-spin interaction. We note that in this limit the resulting spin-spin coupling takes the form of an Ising interaction which, together with single qubit rotations, can be used[4] to efficiently perform CNOT gate operations between two qubits. We finally note that in one dimensions the Rashba interaction can be treated exactly, leading to a renormalization of the g factor,[25] $g\rightarrow g\exp(-\lambda^2/\lambda_{\mathrm{SO}}^2)$. This exact treatment is no longer possible in the 2D case considered here, except for the special case[42] when $\alpha=\pm\beta$ and the problem becomes effectively 1D.[42]

C. Strong Coulomb coupling $\delta\gg1$

We turn now to the more involved case of strong Coulomb interaction strength $\delta\gg1$ which cannot be treated perturbatively. However, some approximations are still possible and we will explore two of them in the following section. The first approximation consists of reducing the two electron system to two classical point-charge particles. The classical equilibrium condition will be obtained by minimizing the total potential energy of the two particles. By doing this, the motion of the electrons will take place around the new equilibrium positions obtained from the equation

$$a^2(a-a_0)=2\lambda^4/a_B, \tag{53}$$

where a_0 is the initial geometric distance and a the effective distance between the electrons in classical equilibrium. However, we are interested in the motion around the equilibrium position, which means that for small deviations, we may substitute the full Coulomb interaction with an effective one, remembering that $\boldsymbol{r}=\boldsymbol{r}_1-\boldsymbol{r}_2$,

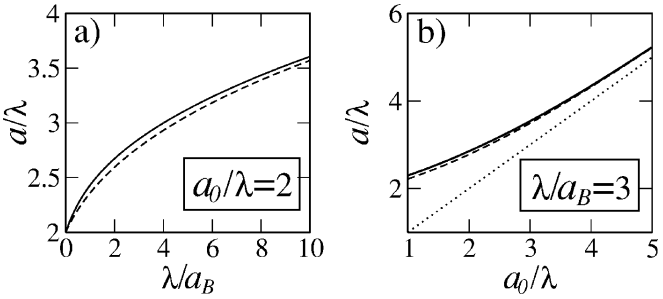

FIG. 3. (a) The effective distance a as a function of the Coulomb interaction strength λ/a_B for $a_0/\lambda=2$. The full line represents the variational result from Eq. (57). The dashed line corresponds to the one obtained from the classical equilibrium solution of Eq. (53). (b) Effective distance a/λ as a function of the geometrical one a_0/λ for $\lambda/a_B=3$. All distances are scaled with the dot radius λ. The dotted line is a_0/λ which is shown for comparison.

$$\frac{e^2}{\kappa|\boldsymbol{r}+\boldsymbol{a}_0|}\rightarrow\frac{e^2}{2\kappa a^3}[3(\boldsymbol{n}_a\cdot\boldsymbol{r})^2-r^2]. \tag{54}$$

We note that the coordinates are measured now with respect to the new equilibrium position. Within this approximation, the relative Hamiltonian H_r is replaced with the new, renormalized one

$$\tilde{H}_r=\frac{p^2}{2m}+\frac{1}{2}m\omega_x^2x^2+\frac{1}{2}m\omega_y^2y^2, \tag{55}$$

with the definition $\omega_{x,y}=b_{x,y}\omega_0$ and $b_{x,y}$ given by the expressions

$$b_x=\sqrt{1+4(\lambda/a_B)(\lambda/a)^3},\quad b_y=\sqrt{1-2(\lambda/a_B)(\lambda/a)^3}. \tag{56}$$

We see that this approximation leads only to a renormalization of the orbital frequencies of the relative Hamiltonian. We proceed now to develop a second alternative for treating the Coulomb interaction, namely a variational method based on the same picture of classical equilibrium. This consists in substituting the full Coulomb interaction term with the same type of expression as in Eq. (53), but with the effective distance obtained from the variational ansatz. For this we minimize the expectation value of the orbital Hamiltonian H_r+H_C, in the ground state of the effective relative Hamiltonian $\tilde{H}_r$ [Eq. (55)] with respect to the effective distance a. This leads to the equation

$$\frac{\partial}{\partial a}\langle\tilde{\psi}_0|H_r+H_C|\tilde{\psi}_0\rangle=0, \tag{57}$$

where $|\tilde{\psi}_0\rangle$ is the ground state belonging to $\tilde{H}_r$, i.e., $\tilde{H}_r|\tilde{\psi}_0\rangle=\tilde{E}_0|\tilde{\psi}_0\rangle$, with $\tilde{E}_0$ the ground state energy. Since we are dealing with harmonic oscillators, those wave functions are known. However, Eq. (57) for the effective distance a can be solved only numerically. We plot in Fig. 3 the results obtained for the effective distance a as a function of different parameters in both cases, namely, the variational result from Eq. (57) and also the result obtained from the classical equilibrium condition in Eq. (53). We see in Fig. 3 that there is

very good agreement between the two approaches in a wide parameter range and moreover, that the effective distance within the variational approach is larger then the one obtained from classical equilibrium, that means a lower ground state energy. We note that a perpendicular magnetic field practically does not change the curves in Fig. 3 (not shown) on a large range of magnetic field strengths ($0<\omega_c<3\omega_0$), which means that the effective distance is to a very good approximation independent of the applied magnetic field. In order to verify the accuracy of our variational method, we checked also the numerical fidelity, defined as the overlap of the wave functions in the variational case with the exact (almost, in the sense of perturbation theory) wave function. Although the problem contains no small parameter, we can still define small matrix elements compared with level spacing in a numerical sense. For this we write the full relative Hamiltonian in the following way:

$$H_r = \tilde{H}_r + V, \tag{58}$$

with the effective Coulomb interaction V [see Eq. (54)] expressed now also in terms of the new equilibrium coordinates [introduced after Eq. (54)],

$$V = \frac{e^2}{\kappa|\boldsymbol{r}+\boldsymbol{a}|} - \frac{e^2}{2\kappa a^3}[3(\boldsymbol{n}_{a0}\cdot\boldsymbol{r})^2 - r^2] + \frac{e^2 x}{\kappa a^2}. \tag{59}$$

We show now that this term leads to small matrix elements so that indeed $|V_{0n}| \ll |\tilde{E}_n - \tilde{E}_0|$, where the energies $\tilde{E}_n$ and $\tilde{E}_0$ are the n-eigenvalue and ground-state energy of the Hamiltonian $\tilde{H}_r$, respectively. To see this numerically we introduce the fidelity

$$F = |\langle\psi_0|\tilde{\psi}_0\rangle|^2, \tag{60}$$

where $|\psi_0\rangle$ and $|\tilde{\psi}_0\rangle$ are the ground state wave functions of the full Hamiltonian H_r and $\tilde{H}_r$, respectively. We now estimate the fidelity F by using perturbation theory to find the true ground-state wave function $|\psi_0\rangle$ from the effective one $|\tilde{\psi}_0\rangle$

$$|\psi_0\rangle = |\tilde{\psi}_0\rangle + \sum_{n=1}^{\infty} \frac{\langle\tilde{\psi}_n|V|\tilde{\psi}_0\rangle}{\tilde{E}_n - \tilde{E}_0}|\tilde{\psi}_n\rangle + \cdots, \tag{61}$$

where we retain only terms to first order in V. Taking into account Eq. (61) we obtain the infidelity $1-F$, namely, the deviation of the true ground state wave function from the effective one

$$1 - F = \sum_{n=1}^{\infty} \left| \frac{\langle\tilde{\psi}_n|V|\tilde{\psi}_0\rangle}{\tilde{E}_n - \tilde{E}_0} \right|^2. \tag{62}$$

We plot in Fig. 4 the infidelity $1-F$ as a function of the effective distance a for fixed Coulomb strength λ/a_B. We see that the infidelity takes very small values ($1-F<10^{-2}$) on the considered range, for two different Coulomb strengths, which shows that our variational approach is very accurate.

We can now evaluate the spin-spin interaction within this approximation. Since we are now dealing with harmonic potentials only, the problem of finding $J_{\tilde{x},\tilde{y}}$ from Eq. (16) becomes straightforward. However, in the derivation of the spin Hamiltonian we need again some relations, similar to Eqs. (22) and (23), but for the present case with the harmonic oscillator renormalized. These relations read

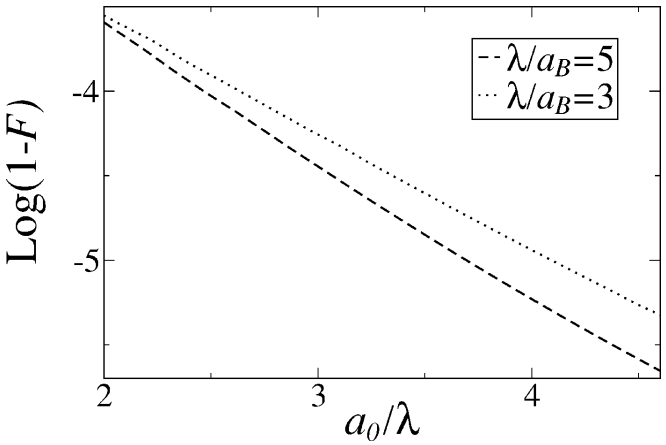

FIG. 4. The logarithm of infidelity $1-F$ from Eq. (62) as a function of the geometric distance a_0/λ (scaled with the dot radius λ) for two different values of Coulomb interaction strength λ/a_B.

$$L_R^{-1}X = -\frac{i}{\hbar M\omega_0^2}\left(P_X + \frac{eB_z}{c}Y\right),$$

$$L_R^{-1}Y = -\frac{i}{\hbar M\omega_0^2}\left(P_Y - \frac{eB_z}{c}X\right), \tag{63}$$

$$L_r^{-1}x = -\frac{i}{\hbar m\omega_x^2}\left(p_x + \frac{eB_z}{c}y\right),$$

$$L_r^{-1}y = -\frac{i}{\hbar m\omega_y^2}\left(p_y - \frac{eB_z}{c}x\right). \tag{64}$$

Making use of the relations (63) and (64), and also with the effective spin-orbit interaction expressed in the center-of-mass and relative coordinates, see Eq. (9), the spin-Hamiltonian H_s takes the form

$$H_s = \frac{E_Z^2}{m^{*2}\omega_0^2\lambda_{\mathrm{SO}}^2}\left[\left(\frac{1}{b_x^2}-1\right)\sigma_x^1\sigma_x^2 + \left(\frac{1}{b_y^2}-1\right)\sigma_y^1\sigma_y^2\right], \tag{65}$$

for the case of a perpendicular magnetic field and

$$H_s = \frac{E_Z^2}{m^{*2}\omega_0^2\lambda_{\mathrm{SO}}^2}\left(\frac{\cos^2\Phi}{b_x^2} + \frac{\sin^2\Phi}{b_y^2} - 1\right)\sigma_{\tilde{y}}^1\sigma_{\tilde{y}}^2, \tag{66}$$

for the case of an in-plane magnetic field which makes an angle Φ with the interdot distance direction. The $\tilde{y}$ is along the in-plane direction perpendicular to the in-plane magnetic field. We see that the spin Hamiltonian depends on the Coulomb interaction part via the difference between the inverse of the renormalized frequencies $\omega_{x,y}$ and the bare one ω_0. As expected, when there is no renormalizations of the bare frequencies (no Coulomb interaction) the interaction vanishes. Referring again to the effective spin Hamiltonian H_s^{eff} from

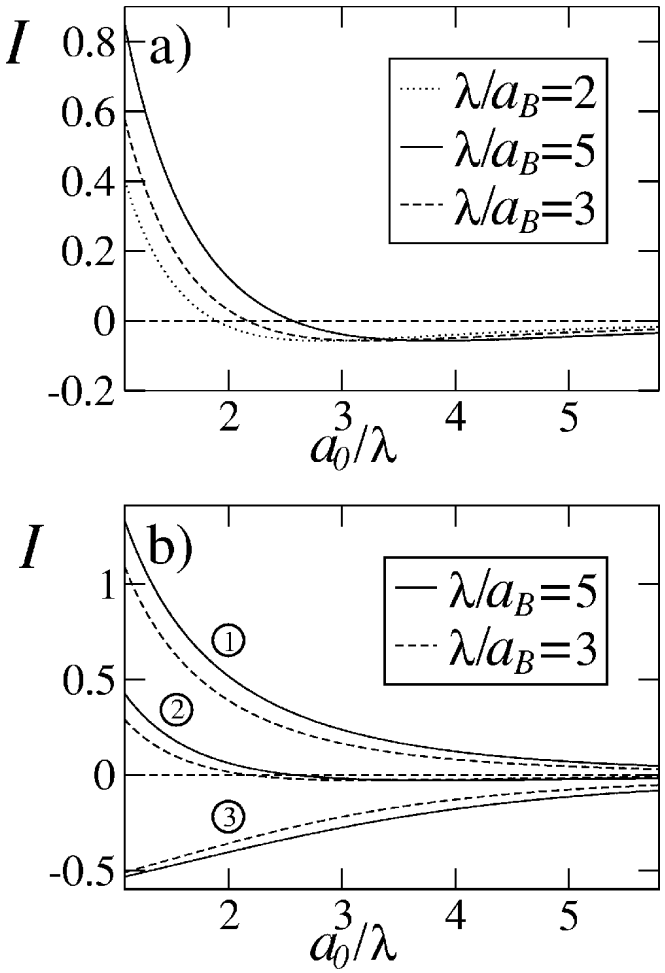

FIG. 5. The function I from Eq. (68) as a function of the dimensionless geometric distance a_0/λ. (a) The case of perpendicular magnetic ($\theta=0$) field for three different Coulomb strength parameters λ/a_B. (b) The case of in-plane magnetic field ($\theta=\pi/2$), for two values of the Coulomb strength λ/a_B, for three angles between the inter-dot distance vector $\boldsymbol{a}_0$ and the magnetic field. The groups of lines 1, 2, and 3 correspond to $\Phi=0$, $\Phi=\pi/4$, and $\Phi=\pi/2$, respectively.

Eq. (19), we obtain for the coupling J_{eff} for arbitrary magnetic field orientations

$$J_{\text{eff}} = E_z \frac{E_z}{\hbar\omega_0}\left(\frac{\lambda}{\lambda_{\text{SO}}}\right)^2 I(a_0/\lambda, a_B/\lambda), \tag{67}$$

where

$$I(a_0/\lambda, a_B/\lambda) = \left(\frac{1}{b_x^2}-1\right)(\cos^2\theta\sin^2\Phi+\cos^2\Phi)+\left(\frac{1}{b_y^2}-1\right)\times(\cos^2\theta\cos^2\Phi+\sin^2\Phi). \tag{68}$$

One can see from Fig. 5(b) that for in-plane magnetic fields one obtains quite large values for I in the two limiting cases $\Phi=0$ and $\Phi=\pi/2$. Changing the magnetic field orientation in-plane one can tune the coupling strength J_{eff} from negative to positive values, i.e., from ferromagnetic to antiferromagnetic regime, and make it vanish for the angle (for in-plane magnetic field)

$$\Phi = \arcsin[b_y\sqrt{(1-b_x^2)/(b_y^2-b_x^2)}]. \tag{69}$$

In the case of a perpendicular magnetic field, see Fig. 5(a), we see that the coupling shows a nonmonotonic behavior as a function of distance a_0, and, moreover, J_{eff} vanishes for some given distance, which for $\lambda/a_B=5$ is about $a_0/\lambda\approx 2.5$. This could be used to tune J_{eff} on and off by changing the distance between the dots.

Next, we consider the case of very elliptic dots, with the bare oscillator frequencies $\omega_{0x,0y}$ corresponding to the x and y directions, respectively, such that $\omega_{0x}\ll\omega_{0y}$. The spin-spin coupling becomes in this limiting case

$$H_s = \frac{E_Z^2}{m^{*2}\lambda_{\text{SO}}^2\tilde{\omega}_x^2}\left(\frac{1}{b_x^2}-1\right)\cos^2\Phi\sigma_x^1\sigma_x^2 + O[(\omega_{0x}/\omega_{0y})^2], \tag{70}$$

where both perpendicular ($\Phi=0$) and in-plane magnetic fields are contained. We see that the problem becomes effectively 1D with an Ising-type spin-spin coupling, similar to the case of small Coulomb coupling studied in the previous section. We mention that for finite ratio of the two bare frequencies ω_{0x}/ω_{0y} the interaction can be varied by changing this ratio, the angle of cancellation defined in Eq. (69) varying as well.

The behavior displayed in Fig. 5 can be understood as follows. The spin-spin coupling is directly related to the deformation of the charge distributions in the two dots as a consequence of the strong Coulomb interaction ($\delta\gg 1$). Thus, the stronger the deformation is, the stronger the spin-spin coupling becomes. Or, in our case, the stronger the deviation of the renormalized orbital frequencies $\omega_{x,y}$ from the bare one ω_0 is, the stronger the coupling becomes, see Eqs. (65) and (66). While the x component of the spin-spin coupling is bounded because the inverse of ω_x tends to zero as the Coulomb interaction strength δ increases, the y component of this coupling is unbounded since the inverse of ω_y can grow indefinitely. Consequently, the y component will dominate the x component for large Coulomb strength and small interdot distance a_0. However, the situation is reversed in the large distance limit, since ω_x increases faster than ω_y decreases as seen from Eq. (56). These opposite limits lead to the nonmonotonic behavior depicted in Fig. 5(a) (perpendicular magnetic field).

We mention that the large distance limit of Eq. (67) converges to the large distance result obtained in the previous section, Eq. (39). However, it does not converge to the results of the previous section in the case of small distance [Eq. (41)], when going from $\delta\gg 1$ to $\delta\ll 1$, a crossover description ($\delta\sim 1$) being needed in this situation. Phrased differently, tuning the spin-spin coupling J_{eff} from strong ($\delta\gg 1$) to small ($\delta\ll 1$) Coulomb interaction regime by varying the interdot distance reproduces the corresponding $\delta\ll 1$ result in Eq. (39), while by varying the ratio λ/a_B does not reproduce the corresponding $\delta\ll 1$ limit, i.e., Eq. (41).

Let us give now some estimates for the coupling J_{eff} when an in-plane magnetic field is applied along, say, the x direc-

tion. Assuming now GaAs quantum dots, and $E_Z=0.1$ meV ($B=4$ T), $\hbar\omega_0=0.5$ meV ($\lambda/a_B\approx 5$), $\lambda/\lambda_{SO}\approx 10^{-1}$. Using these numbers and taking for the geometric interdot distance $a_0/\lambda\approx 2$, we obtain $J_{\rm eff}\approx 10^{-7}$ eV. It is worth mentioning that the hyperfine interaction between the electron and the collection of nuclei in a quantum dot ($\approx 10^5$) leads to similar energy scales.[43,44] This shows that the spin-spin coupling derived here can be very relevant for the spin dynamics in the case of electrostatically coupled quantum dots and that it can also compete with other types of interactions. Considering now the case of InAs quantum dots in a magnetic field along the x direction, with $\lambda_{SO}\approx 2\lambda\approx 100$ nm and $E_Z/\hbar\omega_0=0.1$ and taking also $a_0/\lambda\approx 2$, a value of $J_{\rm eff}\approx 10^{-6}$ eV it is obtained. However, this is just a rough estimate since the spin-orbit coupling cannot be treated as a perturbation anymore and our approximation, being pushed to the limit of its range of validity, starts to break down.

IV. MEASUREMENT SCHEME

In this section we propose a measurement scheme for the spin-spin interaction $J_{\rm eff}$. Similar to the spin relaxation experiments in Ref. 8, the left dot is monitored by a sensitive charge detector, such as a quantum point contact (QPC) or a single electron transistor (SET). We show the main steps of the scheme in Fig. 6.

The first step is the initialization step shown in Fig. 6(a). At low temperatures, $T\ll E_Z$, a single-electron dot will relax to the ground state after a time larger than the spin relaxation time $T_1\simeq(0.1-100)$ ms. A faster spin relaxation can be induced by cotunneling with the lead, for which the dot can be placed closer to the Fermi surface for some time. In Fig. 6(a), the left dot is initialized in the lower Zeeman sublevel $|\uparrow\rangle$, whereas the right dot is empty. Next, the right-dot energy is lowered below the Fermi energy and the dot is quickly filled with an electron in either upper or lower Zeeman sublevel. This is a sequential tunneling process and we denote its rate by Γ. In Fig. 6(b), both dots are deep below the Fermi surface and $J_{\rm eff}$ is the energy scale that governs a coherent evolution in the subspace $\{|\uparrow\downarrow\rangle,|\downarrow\uparrow\rangle\}$. The two spin density matrix reads

$$\varrho(t)=\frac{1}{2}|\uparrow\uparrow\rangle\langle\uparrow\uparrow|+\frac{1}{2}|\Psi(t)\rangle\langle\Psi(t)|, \tag{71}$$

where $|\Psi(t)\rangle$ is the wave function that describes the occurrence of the state $|\uparrow\downarrow\rangle$ in the initialization step. In the ideal case, $|\Psi(t)\rangle$ evolves coherently due to the spin-spin interaction (19)

$$\Psi(t)\rangle=\cos(4J_{\rm eff}t/\hbar)|\uparrow\downarrow\rangle-i\sin(4J_{\rm eff}t/\hbar)|\downarrow\uparrow\rangle. \tag{72}$$

Here, we neglect the cotunneling and other spin relaxation processes. In particular, the cotunneling rate $\Gamma^2/U_\pm$ should be much smaller than the spin-spin coupling $J_{\rm eff}$. Here, $U_\pm$ is the addition/extraction energy of the single-electron quantum dot in the Coulomb blockade valley. On the other hand the sequential tunneling rate Γ should be large enough, so that the spins have no time to evolve during the initialization and measurement steps. We summarize the required regime by the inequality

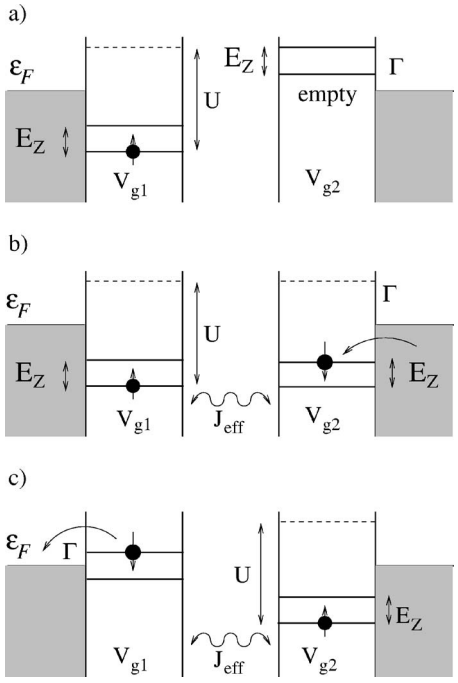

FIG. 6. Scheme to measure the coupling constant $J_{\rm eff}$ in quantum dots without tunnel coupling. In the initialization step (a), the left dot is at equilibrium with one electron in the lower Zeeman sublevel and the right dot is empty. At the start of the coherent evolution step (b), the right dot is filled with one electron in either upper or lower Zeeman level during a short time $\hbar/\Gamma\ll\hbar/J_{\rm eff}$, and the dots are deep in the Coulomb blockade valley $\Gamma^2/U_\pm\ll J_{\rm eff}$. Further, the two spins evolve coherently due to the spin-spin interaction $J_{\rm eff}$ during a fixed time $\tau\gtrsim\hbar/J_{\rm eff}$. In the read-out step (c), the left dot is brought up to the Fermi surface, so that the electron can tunnel to the lead only if it is in the upper Zeeman sublevel. The latter event is recorded by a charge detector nearby the left dot.

$$\frac{\Gamma^2}{U_\pm}\ll J_{\rm eff}\ll\Gamma. \tag{73}$$

After a waiting time τ, the probability of the left-dot electron to be in the upper Zeeman sublevel reads

$$P_{L\downarrow}(\tau)=\frac{1}{4}[1-\cos(8J_{\rm eff}\tau/\hbar)]. \tag{74}$$

Form the period of this function ($\tau_0=\pi\hbar/4J_{\rm eff}$) one can extract the value of the coupling constant $J_{\rm eff}$.

The measurement of the probability $P_{L\downarrow}(\tau)$ can be performed in the same fashion as in Ref. 8. After the waiting time τ, the left dot is brought up to the Fermi level and placed such that the electron can tunnel into the lead only from the upper Zeeman sublevel. This configuration is shown in Fig. 6(c). Tunneling of the electron out and refilling the quantum dot with an electron of the opposite spin is monitored by the charge detector close to the left dot (not shown). For each value of the waiting time τ, the cycle of initialization, coherent evolution, and measurement has to be repeated many times in order to reach a good accuracy.

Next, we remark that the hyperfine interaction with the lattice nuclei should not impede the measurement of $J_{\rm eff}$ as long as $4J_{\rm eff}\gtrsim A/\sqrt{N}$, where A is the atomic hyperfine cou-

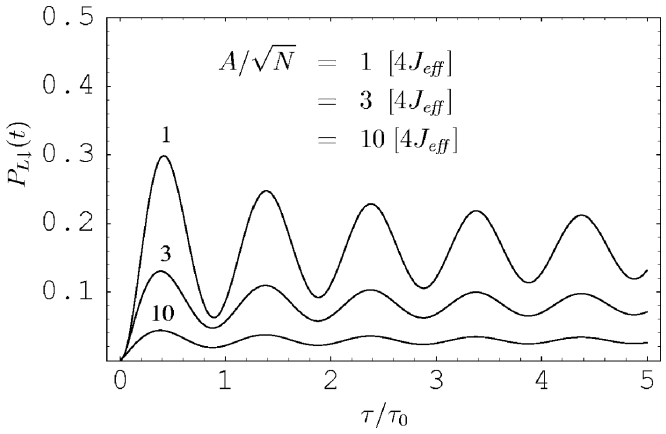

FIG. 7. Residual oscillations in the averaged probability $\bar{P}_{L\downarrow}(\tau)$ for values of $A/\sqrt{N}$ that exceed the spin-spin interaction strength $4J_{\rm eff}$. The period of oscillations is not affected by the hyperfine interaction and is given by $\tau_0=\pi\hbar/4J_{\rm eff}$. With increasing the hyperfine strength $A/\sqrt{N}$, the amplitude of oscillations decreases as $\propto\sqrt{N}/A$. As a function of the waiting time τ, the envelope of oscillations decays as $\propto 1/\sqrt{\tau}$.

pling constant and N is the number of nuclei in both quantum dots. Note that the ratio of $J_{\rm eff}$ to $A/\sqrt{N}$ for a constant λ/a scales with the dot lateral size as $\propto\lambda^4$, for strong Coulomb interaction, and as $\propto\lambda^6$, for weak Coulomb interaction. Therefore, the regime $4J_{\rm eff}>A/\sqrt{N}$ can be easily achieved by taking a larger quantum dot. Furthermore, the hyperfine interaction with the nuclei has only the effect of reducing the visibility of oscillations of $P_{L\downarrow}(t)$, and even for $A/\sqrt{N}\gg J_{\rm eff}$ a small part of $P_{L\downarrow}(\tau)$ shows oscillatory behavior with unchanged period, $\tau_0=\pi\hbar/4J_{\rm eff}$.

In Fig. 7, we plot the probability $P_{L\downarrow}(\tau)$ averaged over the realizations of the hyperfine field. We choose $A/\sqrt{N}\geqslant 4J_{\rm eff}$ to show that the measurement scheme is robust against the hyperfine field. The oscillations are well visible even when $A/\sqrt{N}$ is several times larger than $4J_{\rm eff}$. The averaged probability $\bar{P}_{L\downarrow}(\tau)$ is obtained in the following way. For the subspace $\{|\uparrow\downarrow\rangle,|\downarrow\uparrow\rangle\}$ and in the limit $E_Z\gg A/\sqrt{N}$, the coupling of spins to the hyperfine field is given by $H_{\delta h_z}=\frac{1}{2}\delta h_z(\sigma_1^z-\sigma_2^z)$, where the hyperfine field δh_z has a Gaussian distribution with zero average and a variance $\sigma=A/\sqrt{N}$, which we take to be a measurable parameter that defines N.[45] For more detail on the derivation of $H_{\delta h_z}$ we refer the reader to Ref. 46.

For our description to be accurate, the time between subsequent cycles of initialization, coherent evolution, and measurement should be larger than the nuclear spin relaxation time. Considering the sum of $H_{\delta h_z}$ and $H_s^{\rm eff}$ in Eq. (19), we find that the probability $P_{L\downarrow}(\tau)$ for a fixed value of δh_z is given by[47,48]

$$P_{L\downarrow}(\tau)=\frac{1-\cos(2\tau\hbar^{-1}\sqrt{16J_{\rm eff}^2+\delta h_z^2})}{4(1+\delta h_z^2/16J_{\rm eff}^2)}. \tag{75}$$

The averaged probability $\bar{P}_{L\downarrow}(\tau)$ is then computed by integrating Eq. (75) over δh_z with the Gaussian weight factor $P_\sigma(\delta h_z)=\frac{1}{\sigma\sqrt{2\pi}}e^{-\delta h_z^2/2\sigma^2}$, where $\sigma=A/\sqrt{N}$.

Considering $A/\sqrt{N}>4J_{\rm eff}$ and $\tau>\pi\hbar/4J_{\rm eff}$, we find that the visibility of oscillations scales with $A/\sqrt{N}$ and τ as follows:

$$v\propto\frac{J_{\rm eff}\sqrt{N}}{A}\sqrt{\frac{\hbar}{\tau J_{\rm eff}}}. \tag{76}$$

Note that the scaling law $v\propto\sqrt{N}/A$ is weaker than what one might expect naively from Eq. (75), after substituting there δh_z by its typical value $A/\sqrt{N}$, which gives $v\propto N/A^2$. The reason for the weaker scaling law is the fact that δh_z is centered around zero and the denominator in Eq. (75) has nearly no effect. We find that the numerical results in Fig. 7 can be reproduced fairly accurately, if we approximate the argument of the cosine in Eq. (75) as follows:

$$\sqrt{16J_{\rm eff}^2+\delta h_z^2}\approx 4J_{\rm eff}\left(1+\frac{\delta h_z^2}{32J_{\rm eff}^2}+\cdots\right). \tag{77}$$

This approximation is justified in the regime $\tau\gg\tau_0$ by the the minimal phase requirement, despite the fact that $\delta h_z/J_{\rm eff}$ may be large. With Eq. (77), it is easy to average $P_{L\downarrow}(\tau)$ and obtain an approximate expression, which is fairly accurate for $\tau\gtrsim\tau_0$ and asymptotically exact in the limit $\tau\gg\tau_0$. We thus obtain

$$\bar{P}_{L\downarrow}(\tau)=\frac{1}{4}[\bar{p}-\delta p(\tau)], \tag{78}$$

$$\bar{p}=\sqrt{\frac{\pi}{2}}\zeta\exp\left(\frac{\zeta^2}{2}\right)\mathrm{erfc}\left(\frac{\zeta}{\sqrt{2}}\right), \tag{79}$$

$$\delta p(\tau)=\frac{\zeta\cos[2\pi\tau/\tau_0+\varphi_0(\tau)]}{[\zeta^4+(2\pi\tau/\tau_0)^2]^{1/4}}, \tag{80}$$

where $\zeta=4J_{\rm eff}\sqrt{N}/A$, $\mathrm{erfc}(\zeta)$ is the complementary error function, and the running phase shift $\varphi_0(\tau)$ is given by

$$\varphi_0(\tau)=\frac{1}{2}\arctan\left(\frac{2\pi\tau}{\tau_0\zeta^2}\right). \tag{81}$$

We note that Eq. (78) is exact in two limiting cases: $\zeta\gg 1$ and $\tau\gg\tau_0$. In particular, in the limit $\zeta\to\infty$, we recover $P_{L\downarrow}(\tau)$ in Eq. (75) for all values of τ. In the opposite limit, $\zeta\ll 1$, Eqs. (78)–(81) can be significantly simplified, yielding

$$\bar{P}_{L\downarrow}(\tau)=\frac{\zeta}{4}\left[\sqrt{\frac{\pi}{2}}-\sqrt{\frac{\tau_0}{2\pi\tau}}\cos(2\pi\tau/\tau_0+\pi/4)\right]. \tag{82}$$

V. DISCUSSIONS AND CONCLUSIONS

In the entire derivation we assumed no tunneling between the dots. Even in the presence of tunneling, when direct Coulomb repulsion, U_{12} (which is just the classical interaction

between two charge distributions) is larger than the exchange interaction J_{exc} ($U_{12} \gg J_{\mathrm{exc}}$), the theory presented here is expected to remain still valid. The reason is that this type of spin-spin coupling is a direct consequence of the deformation of the electronic charge distribution due to Coulomb repulsion between the two electrons. Since this is given by the sum of the direct Coulomb part U_{12}, and the exchange part J_{exc}, the spin coupling J_{eff} will be insensitive to exchange in the limit $U_{12} \gg J_{\mathrm{exc}}$. The point now is that with finite tunneling, even with the assumption that the coupling strength J_{eff} is not modified by the exchange Coulomb interaction, the resulting Heisenberg exchange coupling J_{exc} ($H_{\mathrm{exc}}=J_{\mathrm{exc}}\boldsymbol{S}_1\cdot\boldsymbol{S}_2$) will start to compete with the electrostatically induced spin interaction. As a consequence, the spin coupling J_{eff} will be washed out in the limit $J_{\mathrm{exc}} \gg J_{\mathrm{eff}}$. However, since the Heisenberg exchange coupling decays with the interdot distance as[27] $J_{\mathrm{exc}} \sim \exp(-2a_0^2)$ while $J_{\mathrm{eff}} \sim a_0^{-3}$, the electrostatic spin coupling will start to dominate at not very large distances.

We recall that when having exchange, another type of spin coupling $J_{\mathrm{exc}}^{\mathrm{SO}}$, induced by spin-orbit interaction comes into play, and which is proportional to the Heisenberg coupling J_{exc}, i.e., $J_{\mathrm{exc}}^{\mathrm{SO}} \propto (0.1-0.01)J_{\mathrm{exc}}$ for typical GaAs dots.[27,30–34] Thus, $J_{\mathrm{exc}}^{\mathrm{SO}}$ can be much larger than J_{eff} for large enough Heisenberg coupling, with a crossover from this exchange-type to the direct Coulomb-type coupling taking place at some interdot distance. This crossover, however, occurs before we get $J_{\mathrm{exc}} \sim J_{\mathrm{eff}}$, since $J_{\mathrm{exc}}^{\mathrm{SO}}$ is typically 100 times smaller than J_{exc}. To give an estimate, we assume $J_{\mathrm{exc}} \approx 10^{-5}$ eV for $a_0=1$, which gives $J_{\mathrm{exc}} \approx 3.5\times 10^{-8}$ eV for $a_0=2$, implying that $J_{\mathrm{exc}} < J_{\mathrm{eff}}$.

Another important issue is the effect of screening induced by the surrounding electrons in the 2DEG and the metallic gates. As is well known, the screening effect between two charges becomes important for distances exceeding the screening length $\lambda_{\mathrm{scr}} \sim \lambda_{\mathrm{Fermi}}$ (Fermi liquids). However, the screening of bare Coulomb interaction depends strongly on the dimensionality. In 3D the effect of screening is to induce an exponential decay of the bare Coulomb interaction,[49] with the decay parameter λ_{scr}, while in 2D the decay follows a power law ($\sim r^{-3}$ in the large distance limit),[50–53] with λ_{scr} being the relevant length scale. For GaAs, the screening length is around $\lambda_{\mathrm{scr}} \sim \lambda_{\mathrm{Fermi}} \approx 50$ nm. Moreover, additional screening is introduced by the electrodes to gate the dots, due to their metallic character. The finite screening implies then that our theory in fact overestimates the strength of the electrostatically induced spin coupling J_{eff} for distances exceeding this screening length and the results obtained here become just an upper bound on J_{eff} for this limit.

Being highly controllable, the coupling J_{eff} could be used to perform two qubit gates for the realization of quantum computers with electron spins, as proposed in Ref. 4. The switching times range between rather slow ($\sim 10\ \mu$s in GaAs) and reasonably fast (~ 50 ns in InAs). When making use of the standard exchange coupling[4] for switching (with typical switching times of 100 ps in GaAs) the electrostatically induced spin-coupling found here can lead to gate errors. However, this effect can be controlled by choosing the magnetic field direction or strength and/or the interdot distance such that J_{eff} becomes negligibly small [see Eq. (68)].

In the paper we assume perfect harmonic confinement potentials. In reality the dot potential is not harmonic, although quantum dots with potentials close harmonic have been reported. Our spin-spin interaction by no means relies on the harmonicity of the quantum dot potential. We have used the harmonic confinement potential in our model to give analytical expressions which can be used to estimate the magnitude of the effect for realistic structures. We believe that deviations of the confinement from harmonic will lead to corrections to our results, but will not change (i) the a^{-3} scaling at large distances ($a \gg \lambda$) and (ii) the magnitude of the coupling constant.

Finally, an important question is how orbital fluctuations (for example, of the confining energy $\hbar\omega_0$) or in the interdot distance, measured by variation in the electrostatic energy $e^2/\kappa a_0 \equiv E_{\mathrm{el}}$) mediated via spin-orbit coupling lead to fluctuations in the coupling J_{eff} and thus eventually to spin decoherence. The relation between the orbital dephasing time (which is assumed to be known) and the decoherence induced by the spin coupling J_{eff} reads[46]

$$\frac{\tau_\phi^o}{\tau_\phi^s} \sim \left|\frac{\delta J_{\mathrm{eff}}}{\delta(\hbar\omega_0)}\right|^2 + \left|\frac{\delta J_{\mathrm{eff}}}{\delta E_{\mathrm{el}}}\right|^2, \tag{83}$$

where τ_ϕ^o is the orbital dephasing time and τ_ϕ^s the corresponding spin decoherence time. Assuming an orbital dephasing time $\tau_\phi^0 \approx 1$ ns and also the limiting case of touching dots with the same GaAs parameters as before we obtain a spin decoherence time (lower bound) $\tau_\phi^s \approx 10^{-3}$ s. We mention that these two channels, i.e., fluctuations in the size and in the distance between the dots are the most dominant ones for dephasing through J_{eff}. We can conclude then that the incoherent part due to this type of coupling is negligible compared with other types of decoherence mechanisms, e.g., induced by the hyperfine interaction.[43,44,46]

To conclude, we have derived an effective spin-spin interaction between two electrons localized in two quantum dots, spatially separated, induced by the direct Coulomb interaction and mediated by the spin-orbit coupling. This interaction was found to have the form of an anisotropic XY interaction and to be proportional to the Zeeman energy. The spin-spin coupling was studied both in the weak and strong Coulomb interaction limits and for different magnetic field orientations and strengths. The important features are the non-monotonic behavior of this spin interaction for some magnetic field orientations, together with a vanishing of this interaction for particular interdot distances. This effect can be used to manipulate the spin-spin interaction in electrostatically coupled quantum dots by tuning the interdot distance. We proposed a measurement setup which allows one to access this spin-spin coupling experimentally.

ACKNOWLEDGMENTS

We thank D. Stepanenko, G. Burkard, W. A. Coish, and D. Klauser for useful discussions. We acknowledge financial support from the Swiss NSF, the NCCR Nanoscience, DARPA, ONR, and JST ICORP.

APPENDIX: $J_{\tilde{x},\tilde{y}}$ FOR ARBITRARY B FIELDS

In this Appendix we give explicit formulas for the couplings $J_{\tilde{x},\tilde{y}}$ for an arbitrary magnetic field orientation $\boldsymbol{B}=B(\cos\Phi\sin\theta,\sin\Phi\sin\theta,\cos\theta)$ and for both Rashba and Dresselhaus spin-orbit couplings present. These are obtained by diagonalizing the tensor $\bar{\bar{M}}$, which leads to

$$J_{\tilde{x},\tilde{y}}=\frac{E_Z^2}{2}\{(C_1+C_2)\cos^2\theta+(C_1\cos^2\phi+C_2\sin^2\phi - C_3\sin 2\phi)\sin^2\theta\pm\sqrt{[(C_1+C_2)\cos^2\theta+\sin^2\theta(C_1\cos^2\phi+C_2\sin^2\phi-C_3\sin 2\phi)]^2-4(C_1C_2-C_3^2)\cos^2\theta}\}, \quad \text{(A1)}$$

with $\phi=\Phi-\gamma$ [the angle γ is defined after Eq. (9)]. The functions C_i $(i=1,2,3)$ can be expressed in terms of $C_{a_1b_2}=\langle 0|[L_d^{-1}a_1,b_2]|0\rangle$, $a,b=x,y$, i.e.,

$$C_1=\frac{1}{\lambda_-^2}(\sin^2\gamma C_{x_1x_2}+\cos^2\gamma C_{y_1y_2}+\sin 2\gamma C_{x_1y_2}), \quad \text{(A2)}$$

$$C_2=\frac{1}{\lambda_+^2}(\cos^2\gamma C_{x_1x_2}+\sin^2\gamma C_{y_1y_2}-\sin 2\gamma C_{x_1y_2}), \quad \text{(A3)}$$

$$C_3=\frac{1}{2\lambda_+\lambda_-}(\sin 2\gamma(C_{x_1x_2}-C_{y_1y_2})-\cos 2\gamma C_{x_1y_2}). \quad \text{(A4)}$$

These functions can be identified very easily from our formulas derived in the paper. For example, for the case considered in Eq. (28) (weak Coulomb coupling regime) we get

$$C_{x_1x_2}=\frac{\Delta E_C^x}{m^{*2}\lambda^2\omega_0^4}, \quad C_{y_1y_2}=\frac{\Delta E_C^y}{m^{*2}\lambda^2\omega_0^4}, \quad C_{x_1y_2}=0. \quad \text{(A5)}$$

[1] *Semiconductor Spintronics and Quantum Computation*, edited by D. D. Awschalom, D. Loss, and N. Samarth (Springer, Berlin, 2002).
[2] V. Cerletti, W. A. Coish, O. Gywat, and D. Loss, Nanotechnology **16**, R27 (2005).
[3] J. M. Kikkawa and D. D. Awschalom, Phys. Rev. Lett. **80**, 4313 (1998).
[4] D. Loss and D. P. DiVincenzo, Phys. Rev. A **57**, 120 (1998).
[5] A. Imamoglu, D. D. Awschalom, G. Burkard, D. P. DiVincenzo, D. Loss, M. Sherwin, and A. Small, Phys. Rev. Lett. **83**, 4204 (1999).
[6] M. Ciorga, A. S. Sachrajda, P. Hawrylak, C. Gould, P. Zawadzki, S. Jullian, Y. Feng, and Z. Wasilewski, Phys. Rev. B **61**, R16315 (2000).
[7] K. Ono, D. G. Austing, Y. Tokura, and S. Tarucha, Science **297**, 1313 (2002).
[8] J. M. Elzerman, R. Hanson, L. H. Willems van Beveren, B. Witkamp, L. M. K. Vandersypen, and L. P. Kouwenhoven, Nature (London) **430**, 431 (2004).
[9] M. Kroutvar, Y. Ducommun, D. Heiss, M. Bichler, D. Schuh, G. Abstreiter, and J. J. Finley, Nature (London) **432**, 81 (2004).
[10] J. R. Petta, A. C. Johnson, J. M. Taylor, E. A. Laird, A. Yacoby, M. D. Lukin, C. M. Marcus, M. P. Hanson, and A. C. Gossard, Science **309**, 2180 (2005).
[11] C. W. Lai, P. Maletinsky, A. Badolato, and A. Imamoglu, Phys. Rev. Lett. **96**, 167403 (2006).
[12] F. H. L. Koppens, C. Buizert, K. J. Tielrooij, I. T. Vink, K. C. Nowack, T. Meunier, L. P. Kouwenhoven, and L. M. K. Vandersypen, Nature (London) **442**, 766 (2006).
[13] S. Amasha, K. MacLean, I. Radu, D. M. Zumbuhl, M. A. Kastner, M. P. Hanson, and A. C. Gossard, cond-mat/0607110 (unpublished).
[14] V. I. Mel'nikov and E. I. Rashba, Sov. Phys. JETP **34**, 1353 (1972).
[15] M. Dobrowolska, A. Witowski, J. K. Furdyna, T. Ichiguchi, H. D. Drew, and P. A. Wolff, Phys. Rev. B **29**, 6652 (1984).
[16] G. Salis, Y. Kato, K. Ensslin, D. C. Driscoll, A. C. Gossard, and D. D. Awschalom, Nature (London) **414**, 619 (2001).
[17] E. I. Rashba and Al. L. Efros, Appl. Phys. Lett. **83**, 5295 (2003).
[18] M. Duckheim and D. Loss, Nat. Phys. **3**, 195 (2006).
[19] V. N. Golovach, M. Borhani, and D. Loss, Phys. Rev. B **74**, 165319 (2006).
[20] A. V. Khaetskii and Yu. V. Nazarov, Phys. Rev. B **64**, 125316 (2001).
[21] V. N. Golovach, A. Khaetskii, and D. Loss, Phys. Rev. Lett. **93**, 016601 (2004).
[22] M. Borhani, V. N. Golovach, and D. Loss, Phys. Rev. B **73**, 155311 (2006).
[23] A. Abragam, *Principles of Nuclear Magnetism* (Oxford University Press, Oxford 1961).
[24] N. Zhao, L. Zhong, J.-L. Zhu, and C. P. Sun, Phys. Rev. B **74**, 075307 (2006).
[25] C. Flindt, A. S. Sorensen, and K. Flensberg, Phys. Rev. Lett. **97**, 240501 (2006).
[26] To distinguish between the two mechanisms we refer to the coupling studied in this work as "spin-spin coupling" as opposed to the Heisenberg exchange coupling.
[27] G. Burkard, D. Loss, and D. P. DiVincenzo, Phys. Rev. B **59**, 2070 (1999).
[28] X. Hu and S. Das Sarma, Phys. Rev. A **61**, 062301 (2000).
[29] J. Schliemann, D. Loss, and A. H. MacDonald, Phys. Rev. B **63**,

085311 (2001).
[30] K. V. Kavokin, Phys. Rev. B **64**, 075305 (2001).
[31] N. E. Bonesteel, D. Stepanenko, and D. P. DiVincenzo, Phys. Rev. Lett. **87**, 207901 (2001).
[32] G. Burkard and D. Loss, Phys. Rev. Lett. **88**, 047903 (2002).
[33] D. Stepanenko, N. E. Bonesteel, D. P. DiVincenzo, G. Burkard, and D. Loss, Phys. Rev. B **68**, 115306 (2003).
[34] D. Stepanenko and N. E. Bonesteel, Phys. Rev. Lett. **93**, 140501 (2004).
[35] G. Dresselhaus, Phys. Rev. **100**, 580 (1955).
[36] Y. Bychkov and E. I. Rashba, J. Phys. C **17**, 6039 (1984).
[37] N. F. Johnson and M. C. Payne, Phys. Rev. Lett. **67**, 1157 (1991).
[38] V. Fock, Z. Phys. **47**, 446 (1928).
[39] C. G. Darwin, Proc. Cambridge Philos. Soc. **27**, 86 (1930).
[40] D. V. Bulaev and D. Loss, Phys. Rev. B **71**, 205324 (2005).
[41] O. Dippel, P. Schmelcher, and L. S. Cederbaum, Phys. Rev. A **49**, 4415 (1994).
[42] J. Schliemann, J. C. Egues, and D. Loss, Phys. Rev. Lett. **90**, 146801 (2003).
[43] A. V. Khaetskii, D. Loss, and L. Glazman, Phys. Rev. Lett. **88**, 186802 (2002).
[44] W. A. Coish and D. Loss, Phys. Rev. B **70**, 195340 (2004).
[45] More rigorously, $\sigma = IA/\sqrt{2N_0}$, where $I^2 = \langle I_z^2 \rangle$ is the variance of the z component of a single nuclear spin (assuming $\langle I_z \rangle = 0$) and $1/N_0 = v_0 \int d^3r |\psi(\boldsymbol{r})|^4$, with $\psi(\boldsymbol{r})$ being the electron wave function and v_0 the unit cell volume per nuclear spin.
[46] W. A. Coish and D. Loss, Phys. Rev. B **72**, 125337 (2005).
[47] D. Klauser, W. A. Coish, and D. Loss, Phys. Rev. B **73**, 205302 (2006).
[48] We can identify $P_{L\downarrow}(\tau)$ with $[1 - C_{XX}(\tau)]/2$ and J_{eff} with $J/4$ in Ref. 47.
[49] D. Pines and P. Nozieres, *The Theory of Quantum Liquids* (Benjamin, New York, 1966), Vol. 1.
[50] F. Stern, Phys. Rev. Lett. **18**, 546 (1967).
[51] T. Ando, A. B. Fowler, and F. Stern, Rev. Mod. Phys. **54**, 437 (1982).
[52] C. W. J. Beenakker and H. van Houten, in *Solid State Physics: Advances in Research and Applications*, edited by H. Ehrenreich and D. Turnbull (Academic, New York, 1991), Vol. 44, pp. 1–228.
[53] D. S. Saraga and D. Loss, Phys. Rev. B **72**, 195319 (2005).